Manuscript

ANALYSIS OF TRIPOD SUPPORTED OFFSHORE WIND TURBINES UNDER CONDITIONS OF MARINE GROWTH

Francesco Arcigni[1*], K. A. Abhinav[2], Maurizio Collu[2], Mauro Venturini[1]

[1] Dipartimento di Ingegneria, Università degli Studi di Ferrara, Via Giuseppe Saragat, 1, 44122 - Ferrara (Italy)

[2] Department of Naval Architecture, Ocean & Marine Engineering, University of Strathclyde, 100 Montrose Street, Glasgow G4 0LZ, United Kingdom

* Corresponding author: Francesco Arcigni

Dipartimento di Ingegneria, Università degli Studi di Ferrara

Via Giuseppe Saragat, 1, 44122 - Ferrara (Italy)

email address: francesco.arcigni1@gmail.com

ABSTRACT

Offshore wind turbines are now a mature technology to produce renewable energy on a vast scale, nonetheless several design and maintenance planning challenges remain. There have been attempts to investigate the impact of marine growth on fixed offshore wind turbine structures, but only few adopted a whole dynamics approach. This work presents a methodology to capture the influence of marine growth on the dynamic response of a tripod substructure, supporting the NREL 5 MW reference offshore wind turbine, under combined dynamic loads from wind and waves, and including soil-structure interaction by means of the spring-to-ground model. Marine growth is modelled as prescribed by DNV and API, evaluating the effects of variation of its thickness, roughness, and distribution. It is here demonstrated that marine growth thickness and roughness impact significantly on the loads acting on wind turbines' structures and its dynamic response, and that heterogeneity in marine growth thickness profiles vs depth available in literature lead to substantially different results. Tower top displacement becomes 24% higher when marine growth thickness grows from 0 to 200 mm. On the other hand, the changes in the natural frequencies of the support structure with an increase of marine growth's thickness are almost negligible (0.3%).

Keywords: Offshore wind turbine, Marine growth; Tripod offshore support structure; Soil-structure interaction; Dynamic analysis.

NOMENCLATURE

[C]	Damping matrix
[K]	Stiffness matrix
[M]	Mass matrix
{F(t)}	External force vector
C_D	Drag coefficient
C_M	Inertia coefficient
D	Diameter or typical cross section dimension
dS	Infinitesimal surface
dV	Infinitesimal volume
H_s	Significant wave height
k	Stiffness
m	Mass
TI	Turbulence intensity
T_p	Peak spectral period
u	Water particle velocity
U	Wind speed
u’	Water particle acceleration
X	Displacement vector
γ'	Submerged unit weight of soil
ρ	Density
Φ	Angle of internal friction

Acronyms

API	American Petroleum Institute
BEM	Blade Element Momentum
DNV	Det Norske Veritas
FE	Finite Element
FFT	Fast Fourier Transformation
HHT-α	Hilber–Hughes–Taylor-α
ISUM	Idealized Structural Unit Method
K-C	Keulegan-Carpenter
MG	Marine Growth
NREL	National Renewable Energy Laboratory
OC3	Offshore Code Comparison Collaboration
OT	Overturning Moment
OWT	Offshore Wind Turbine
SD	Standard Deviation
SSI	Soil-Structure Interaction

1. INTRODUCTION

1.1 Context

Offshore wind harvesting is one of the most promising technologies in the renewable energy sector [1]. Just in 2019, offshore wind turbines (OWTs) for a record total capacity of 3627 MW have been installed and connected to the grid in Europe. This figure is 30% more than 2018 installed rated power [2]. However, offshore wind exploitation poses more design problems and additional expenses than onshore wind turbines. Costs are mainly represented by support structure and the turbine. Depending on the type of sub-structure, its cost can range from 15% (monopiles) up to 33% (jacket) of the total capital cost [3].

1.2 Problem statement and aim

OWT support type mainly depends on the depth at which it has to operate. However, deeper seas require the adoption of more complex structures, such as tripod or jacket, which can bear more severe sea states using less material, being more structurally efficient [4]. An additional factor to be considered for the design of OWTs is the presence of sea water fauna and vegetation. Marine growth (MG) is defined as the marine organisms that naturally colonize the underwater parts of offshore substructures. Its quantity is influenced by multiple factors, including sea water characteristics, marine current, and geographical location. In addition to corrosion problems, several studies have noted that marine growth influences the structure properties and the wave loads acting on it [5, 6]. The additional weight added around the support braces alters the mass-related properties, such as the natural frequencies (these will be lowered, in general). Moreover, the larger projected area of the structures' members causes higher waves and current loads. Finally, the drag coefficient is incremented by marine growth roughness. In order to optimize the operation and maintenance of these assets, a more in-depth knowledge of marine growth behaviour and its influence on the structure is required.

Although recognised as a potential problem for OWT support structures, at the moment the studies on the effect of marine growth on the dynamic response of tripod are relatively few – and the present work aims at bridging this gap.

1.3 Previous work

Marine growth impact assessment is included in all major offshore structure design codes, such as Det Norske Veritas (DNV) [7]. However, the majority of the studies treat it only as a parameter to take into account when calculating the hydrodynamic coefficients. Detailed experimental studies have been conducted on tubular structures to assess the variation of the hydrodynamic coefficients in the

presence of marine growth [8, 9]. The work done by Sarpkaya *et al*. [10] has been taken into consideration for high values of Keulegan-Carpenter (K-C) number, where the dependency of mass and drag coefficients from K-C is displayed for values till K-C=100.

A comprehensive analysis on marine growth influence on the dynamic response of an OWT supported by a jacket has been conducted by Fevåg [5]. The impact of different marine growth thicknesses has been evaluated, also assessing section-wise distributions of thickness along the depth and on the single members. The variation of hydrodynamic forces and natural frequencies was studied, and a fatigue damage assessment on the structure's braces was conducted. However, only one sea state was considered for determining the environmental loads. Shi *et al*. [6] performed a study on the sensitivity of different marine growth parameters on the response of a jacket type OWT. The paper presents a dynamic response analysis for two different turbine configurations and their operational environmental conditions. The varying parameters are thickness, density, drag, and inertia coefficients. The selection of the evaluated range of values was not justified by literature prescriptions: the paper assesses the influence of a certain range of values around the prescribed ones. Carswell and Arwade [11] produced a comprehensive analysis on the effects of biofouling on a monopile supporting the NREL 5 MW OWT. Both hydrodynamic load enhancement and the impact on natural frequencies have been evaluated. In addition, a range of drag and inertia coefficients have been simulated. Just one regular wave load condition was considered. Moreover, comparing just the 0 mm and 200 mm thickness scenarios leave out the intermediate phases of biofouling growth.

OWT foundations play a big role in the overall dynamic response of the structure. Various methods for modelling the soil-structure interaction (SSI) have been proposed. One of the most used methods to model the lateral load on piles is the non-linear springs method [12]. Herein, the soil is replaced with a number of springs along the pile to replicate its behaviour by setting appropriate stiffness values. The topic of the soil influence on a monopile type offshore wind turbine has been widely treated by Bisoi and Haldar [13], and Abhinav and Saha [12], presenting the dynamic analysis of 2 MW and 5 MW OWTs, respectively, for soil characteristics varying from stiff to soft clay. Abhinav and Saha [14] investigated the influence of sandy soil on a pile supported jacket OWT over a range of environmental load conditions. These studies, however, do not consider the effect of biofouling.

Therefore, the present work focuses on investigating the response of a tripod supporting the NREL 5 MW OWT under combined aerodynamic-hydrodynamic loading, in the presence of marine growth, within a finite element (FE) framework. A water depth of 45 m is considered. Thickness of the marine growth is assumed to vary from 0 mm to a maximum of 200 mm. Loose sandy soil is considered in the study and the soil properties are represented by means of p-y, t-z and Q-z curves. Statistical uncertainty due to the modelling of turbulent wind and irregular wave time series is addressed by means of a probabilistic framework.

93 The methodology adopted in the present work, along with the numerical tools used, is described in Section 2. The modelling
94 parameters and the field of application of this study are discussed in Section 3. The results of the study are presented in Section 4 and
95 the paper concludes with section 5.
96
97 *1.4 Paper's novelty*
98 Studies on the effect of biofouling on monopiles and jacket-type support structures can be found in literature. Tripod-type structures
99 have been examined from several point of view. However, no relevant reference for comprehensive studies on marine growth effects on
100 tripods has been produced yet.
101 The goal of this paper is to perform an investigation on the influence of marine growth on the dynamic performance of the tripod
102 supported OWT, under conditions of combined aerodynamic and hydrodynamic loading, considering the soil-structure interaction (SSI).
103 The aim is to give a complete overview of the problem, highlighting which aspects need further studies to produce reliable results.
104 The literature survey presented in Section 1.3 showed that current studies do not take into consideration both marine growth modelling
105 parameters and multiple sea states for their analyses. Therefore, an aero-hydrodynamic-geotechnical analysis is here attempted. In order
106 to do so, met-ocean conditions have been derived based on probabilistic formulations defined for the North Sea, coupling wind speeds
107 and sea-states, represented by a significant wave height and a peak spectral period. This is essential for a wind turbine dynamic analysis,
108 and this paper makes use of a formulation published in literature, for the same. This procedure has been followed widely in the study of
109 both fixed and floating offshore wind turbines [15].
110 Moreover, a consolidated soil-structure interaction modelling methodology enhances the accuracy of the results also for the natural
111 frequency analysis along with the tower response frequency spectra.
112
113 **2. METHODOLOGY**
114 The dynamics of fixed-to-seabed OWT structures requires the modelling of the aerodynamics loads, the hydrodynamic loads, the
115 structural dynamics of the flexible elements, the soil-structure interaction dynamics, and the control system strategy. The approach
116 proposed here consists in combining these dynamic effects, which act simultaneously. A time-domain approach is adopted in order to
117 take into account these nonlinear loads.
118
119 *2.1 Aerodynamic loading*

Stochastic, three-dimensional turbulent wind fields are generated using NREL's TurbSim code [16], which makes use of the SANDIA method [17]. Herein, a suitable description of the wind speed turbulence spectrum is initially assumed (for instance, the Kaimal spectrum). Wind velocity vector time series are then realized at discrete points in a two-dimensional plane enclosing the wind turbine rotor and tower, using FFT (Fast Fourier Transformation). Using Taylor's frozen turbulence hypothesis, the grids of time histories are marched at the mean wind speed, in the mean wind direction. Wind shear has been considered with the default TurbSim power law model. The power law exponent has been set to 0.14 [16].

NREL's FAST (Fatigue, Aerodynamics, Structures, and Turbulence) code [18] performs a linear interpolation on the full field wind data to determine the velocity components on the blade element locations. The blade element momentum (BEM) approach [19] is adopted to determine the aerodynamic forces acting on the wind turbine blades. The underlying assumption in the BEM theory is that the total aerodynamic force on a blade can be obtained by the summation of the component forces acting on the discrete blade elements [20]. Furthermore, tip losses and hub losses have been taken into account with the Prandtl tip-loss and hub-loss model. Aerodynamic stall has been considered as well [20], instead tower shadow effect option has not been enabled.

2.2 Hydrodynamic loading

Both FAST and the finite elements code USFOS [21] make use of the Morison equation [22] to compute the wave loads acting on the tripod. Herein, the total wave load is obtained as the sum of drag and inertia components, attributed to water particle velocity and acceleration, respectively. As per the Morison equation, the hydrodynamic load, in a direction perpendicular to the cylinder axis, on the infinitesimal length of a cylindrical member is given by:

$$dF = \frac{1}{2}\rho C_D |u| u \, dS + \rho C_M \dot{u} \, dV \tag{1}$$

Here, ρ is the density of water, dS and dV are, respectively, the infinitesimal surface and volume of the cylindrical section, and u is the velocity normal to the cylinder longitudinal axis (therefore $\dot{u}$ is the normal acceleration). C_D and C_M (C_M =1+C_A, C_A being the added mass coefficient) are the drag and inertia coefficients. Irregular sea-waves are generated from the JONSWAP wave spectrum (a peak-enhanced Pierson-Moskowitz spectrum), by means of a constant-area discretization method [23].

2.3 Structural dynamics

For a tripod under wind and wave loading, the dynamic response may be analysed using the following equation:

148 $$M[\ddot{X}] + C[\dot{X}] + K[X] = \{F(t)\} \quad (2)$$

149

150 Here, [M], [C] and [K] are, respectively, the mass, damping and stiffness matrices. X is the displacement vector, and its derivatives
151 represent velocities and accelerations. {F(t)} is the external force vector, sum of hydrodynamic (inertia and drag forces, Section 2.2)
152 and aerodynamic loads (Section 2.1). Numerical time integration is made by means of the Hilber–Hughes–Taylor-α (HHT-α) method,
153 a variation of the Newmark-β method. Here, α is a parameter that indicates the time averaging of the stiffness, damping and load terms
154 [24].

155

156 *2.4 Soil modelling*

157 The tripod is fixed to the seafloor by means of piles embedded into the seabed. Piles refer to hollow cylindrical elements that transfer
158 lateral loads onto the surrounding soils. Detailed information on the load transfer mechanism of offshore piles are well documented in
159 literature ([25, 26]). For the present work, a Winkler spring model is used to model the SSI in the numerical program USFOS. Herein,
160 soil properties are represented by springs attached to the pile at discrete points, along its length, in both lateral and axial directions. Of
161 particular importance for OWT structures are the *p-y* springs that represent the resistance of the soil to lateral loading. Similarly, the *t-z*
162 and *Q-z* curves are used to model the skin friction and tip bearing resistance respectively. The use of springs to model the SSI for
163 offshore structures has been recommended by the design codes - DNV [7] and API (American Petroleum Institute) [27].

164

165 *2.5 Statistical uncertainty*

166 The use of random phases or seeds to generate time histories of wind and wave loading inevitably results in the statistical uncertainty,
167 which is epistemic in nature. This uncertainty can be reduced by increasing the number of time domain simulations, for the same met-
168 ocean condition, but using different wind and wave time series, and averaging across the ensemble to obtain a reliable estimate of the
169 statistical parameters [28]. In the present work, each met-ocean condition is analysed using 20 different wind and wave time histories.
170 This number of seeds aims to represent a trade-off between the choice of one of the main reference studies [14] and a lower computational
171 time. As the reference, the analyses are run for 600 s of simulated time. The total length of each single simulation is 720 s, but the initial
172 120 s are discarded to account for start-up and transient events [29]. The integration time step for the analysis made in USFOS is 0.04
173 s.

174

175

176 *2.6 Combining aerodynamic and hydrodynamic loads*

177 Accurate prediction of the dynamic response of an offshore wind structure can be realized by means of fully coupled simulations.
178 This approach simultaneously accounts for aerodynamics, hydrodynamics, structural dynamics, control dynamics and soil-structure-
179 interaction. However, in several cases, for instance – when the code is lacking the capabilities to perform a fully coupled simulation or
180 because of intellectual property concerns (when turbine control system algorithms cannot be shared between design partners), a semi-
181 coupled approach [30,31], is adopted.

182 This is usually followed in the design of offshore wind foundations, where wind turbine manufacturers (WTM) and foundation
183 designers (FD) perform their own simulations with aeroelastic and geotechnical engineering tools, respectively. There is constant
184 information interchange between the two sets of designers (loads at the mudline are passed from the WTM to the FD, for instance) and
185 the result is an integrated multi-disciplinary design approach [32].

186 For bottom fixed OWTs, a semi-coupled analysis accounting for the aerodynamic and hydrodynamic load effects can give
187 conservative measures of structural response, provided the natural period of the tripod is less than the incoming wave periods's range
188 ([33, 31]). The present work employs a two-stage approach for combining the influences of the wind and wave loads, as illustrated in
189 Figure 1.

190 The first stage involves using FAST for an aero-hydro-servo-elastic analysis on the tripod, fixed at the mudline, to generate the time
191 series of wind loads at the hub of the OWT. In the second stage, these wind load time series are incorporated into the USFOS [21] model
192 of the OWT structure (including the soil domain and marine growth), to constitute a semi-coupled aerodynamic-hydrodynamic-
193 geotechnical analysis. For a semi-coupled approach to be valid, it is necessary for both numerical codes to have similar wave generation
194 capabilities ([33, 29]).

195 In the second stage, the combined dynamic analysis, which includes SSI, is performed using USFOS, a FE program for framed
196 offshore structures such as jackets and tripods. USFOS makes use of a nonlinear FE technique called the Idealized Structural Unit
197 Method (ISUM) [34], which aims to reduce the computational costs by using fewer elements and degrees of freedom [35]. In ISUM,
198 each element in the actual structure is represented using a FE [24]. A Green strain formulation is used [21], which accounts for membrane
199 effects in tubular elements and column buckling.

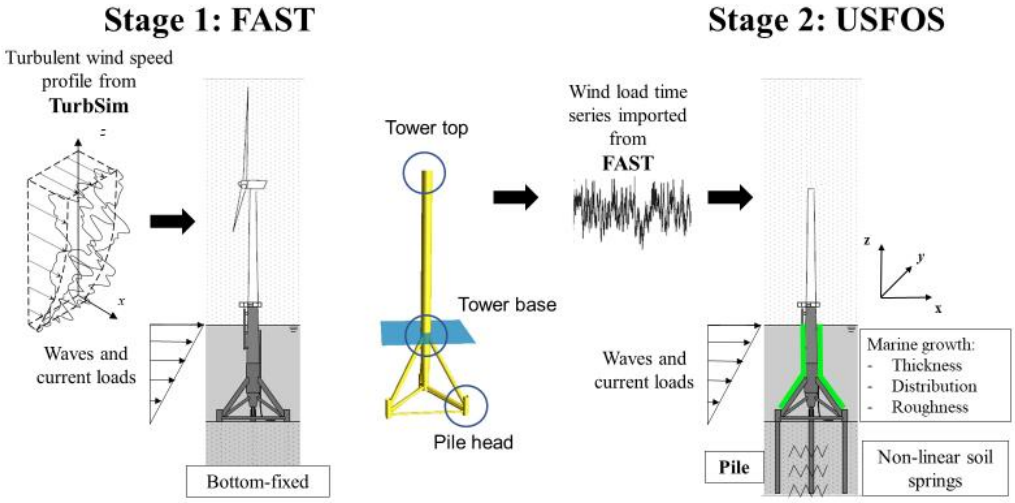

Figure 1 – Scheme of the adopted two-stage procedure

3. CASE STUDY

3.1 Support structure

In the present study, the NREL 5 MW OWT is supported on a tripod substructure. Like a jacket, a tripod is a space frame structure with 3 legs resting on pile foundations. The tripod considered in the study is similar to the one used in the Offshore Code Comparison Collaboration (OC3) project [16]: the water depth is 45 m and the OWT hub is at a height of 87.6 m above the mean sea level. The FE model of the tripod is initially generated in GeniE [36] and is then exported to USFOS. The material considered is steel and its main properties are summarised in Table 1.

Table 1 – Structure's material main properties

Young's Modulus [GPa]	Yield Stress [MPa]	Density [kg/m^3]	Thermal Expansion Coefficient [m/°C]
210	360	7850	1.2 x 10^{-5}

3.2 Metocean conditions

Four metocean conditions have been considered in the present study, as shown in Table 2. Wind velocities have been set; then, consequent sea states have been obtained. Considering the turbine operating wind speed range going from 3 to 25 m/s [4], 6 and 24 m/s scenarios are close to the cut-in and cut-out wind conditions. 12 m/s has been selected as representative of the wind speed range where the maximum energy is extracted. 45 m/s wind speed has been chosen as the extreme speed from Abhinav and Saha [14]. Northern North Sea conditions are assumed, and sea states correlated on wind speed are obtained using a probabilistic formulation proposed by Johannessen *et al*. [37]. Here, U refers to the wind speed at the hub-height, H_s is the significant wave height, T_p is the peak spectral period and TI is the turbulence intensity.

Table 2 – Met-ocean conditions of the study

Load case	***U* [m/s]**	**H_s [m]**	**T_p [s]**	***TI***	**Remarks**
1	6	2.2	9.8	0.20	Below rated wind speed
2	12	3.1	10.1	0.15	Near rated wind speed
3	24	5.7	11.2	0.12	Above rated wind speed
4	45	11.2	13.5	0.10	Extreme wind speed – parked condition

3.3 Soil profile

The soil profile used in the study is given in Table 3. The soil can be classified as loose sand, on the basis of the angle of internal friction (Φ) [38]. Also, the submerged unit weight of soil (γ') is presented in Table 3. These parameters are used to define the type of soil, hence needed for *p-y*, *t-z* and *Q-z* curves.

Piles are modelled below the mudline with a total of 13 nodes, obtaining a total length of 37 m.

Table 3 – Soil profile at the site of the study

Depth [m]	**Type**	**γ' [kN/m^3]**	**Φ [°]**
0.0 – 10.0	Sand	8.25	20
10.0 – 28.0	Sand	9.00	25
28.0 – 37.0	Sand	9.50	30

3.4 Marine growth

Marine growth has been modelled by specifying its thickness (uniform or with different distribution along the water depth), and roughness (through C_D and C_M imposition). The values chosen are summarised in Table 4.

Table 4 – Summary of marine growth modelling parameters

Uniform Thickness [mm]				
0	50	100	150	200
Distribution				
J. Wolfram [39]	DNV [7]	MID [40]	Oldfield [41]	
Roughness				
C_D=0.7 - C_M=2 (Default USFOS C_D and C_M)	Smooth structure members ($k/D < 10^{-4}$)	5 mm	50 mm	

3.4.1 Thickness

A total of five values of constant thickness along the depth has been selected for the analysis. Even though such a condition is unrealistic, this represents the simplest way of assessing the influence of the marine growth presence. Maximum value and thickness increment have been chosen accordingly with the studies taken as reference [5,6]: the outcomes can be directly compared to the majority of the studies on this subject (as made by Fevåg [5]). Being this an unrealistic condition, selecting five main scenarios has been considered a conservative choice, in line with previous studies (such as Fevåg [5]). The references for the thickness values regard a North Sea submarine environment ([9, 42]).

3.4.2 Distribution

Marine growth thickness profiles along the depth have been taken from previous studies involving North Sea scenarios. Distributions are shown in Figure 2, where the thickness profiles have been normalised using the maximum value for a better graphical representation. These profiles have been then scaled to 200 mm, to compare them with the same maximum value. Even though the single maxima were quite different, the purpose of this operation has been to obtain realistic thickness profiles for the simulations. It can be noticed that the trends are quite heterogenous, meaning a different amount of additional mass to the structure and increased hydrodynamic loads. The problem is taken into account during the results discussion.

3.4.3 Roughness

As biofouling grows around smooth steel tubular structures, inertia and drag coefficients change. Both the larger diameter and the higher roughness of the outer surface change the drag force acting on the structure. Inertia coefficient also depends on roughness. Curves that are normally used to estimate these coefficients with Keulegan-Carpenter and Reynolds numbers shift as relative roughness k/D (being k the roughness and D the element's diameter/typical cross section dimension) increases [10]. Previous works have considered just one value for mass and drag coefficient (C_D=0.7, C_M=2.0) for the whole structure [14, 43]. Here, roughness effect has been simulated by calculating drag and inertia coefficients depending on: sea state, K-C number and depth. Depending on these parameters, the hydrodynamic coefficients have been obtained as indicated by DNV and Sarpkaya *et al*. [10]. The latter has been observed for high K-C numbers. As a simplification, the significant wave height and the peak period have been used as inputs to obtain the coefficients. Roughness values have been set as prescribed from DNV [44]: k=5x10^{-2} m and k=5x10^{-3} m (maximum and minimum values of the prescribed range for marine growth). A scenario considering smooth structure elements ($k/D < 10^{-4}$ [44]) has been simulated as well for comparison. Simulations with the default values set in USFOS, which correspond to the DNV [44] recommendation for the smooth surface cases, have been run.

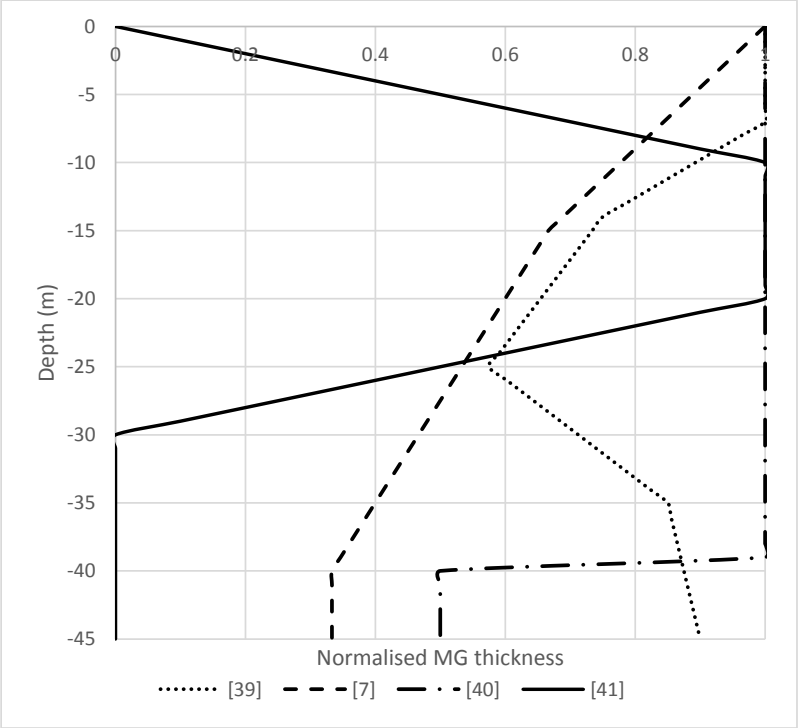

Figure 2 – Marine growth distribution profile along the depth in the considered four scenarios

4. RESULTS AND DISCUSSION

In order to take into account the stochastic nature of the wind and wave loads, the considerations presented below are based on the average over 20 time series realisations (derived from the 20 seeds).

Two types of results will be discussed. The first part will focus on the mean and standard deviation (SD) values of the following dynamic response parameters:

- effect of the variation of MG thickness on tower displacement, horizontal wave load, base shear (the lateral force at the base of the structure) and overturning moment (an estimate of the external forces multiplied by the distance from the soil).
- effect of the variation of MG thickness on the horizontal wave load, considered the most representative hydrodynamic load.
- effect of the variation of MG thickness on the base shear.

The second part will instead investigate the oscillatory response of the structure, from a frequency point of view, as MG thickness increases, showing:

- Comparison between natural and exciting frequencies.
- Response frequency spectra.

4.1 Marine growth parameters variation

4.1.1 Uniform Thickness

Tower displacement

Figure 3 displays the mean lateral (x-direction) displacement along the tower height. The x-axis scale has been exaggerated to allow a better visualisation of the response. The values are increasing along the height, as expected due to the action of the aerodynamic thrust acting at the hub level. On the other hand, a clear monotonic trend when augmenting the marine growth thickness cannot be identified.

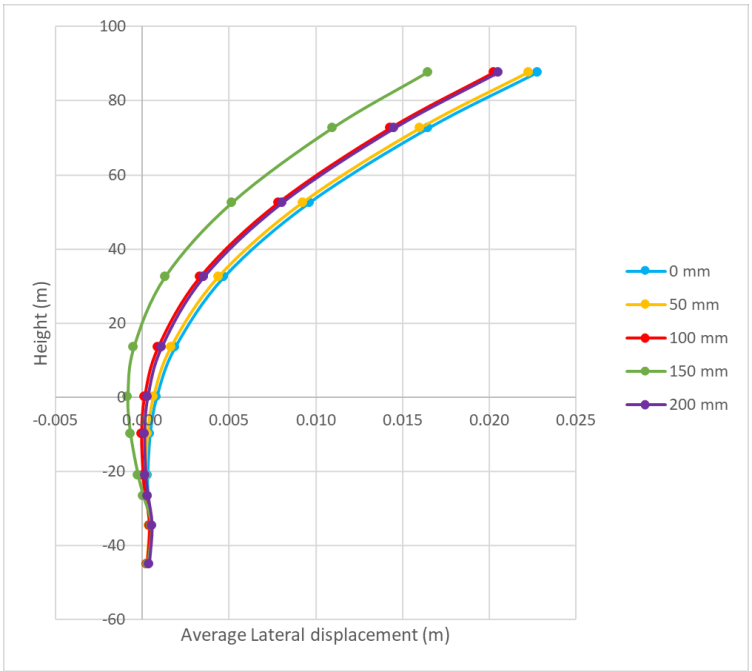

294

295 **Figure 3** – Mean along-height lateral displacement for 5 different marine growth thickness values at sea state corresponding to 12 m/s

296 Due to the oscillatory nature of the wave loads, in addition to the mean value, the standard deviation of the horizontal displacement
297 is also presented in Figure 4. A larger gap between the mean+SD and mean–SD values can be observed, and it is in general proportional
298 to the marine growth thickness.

299

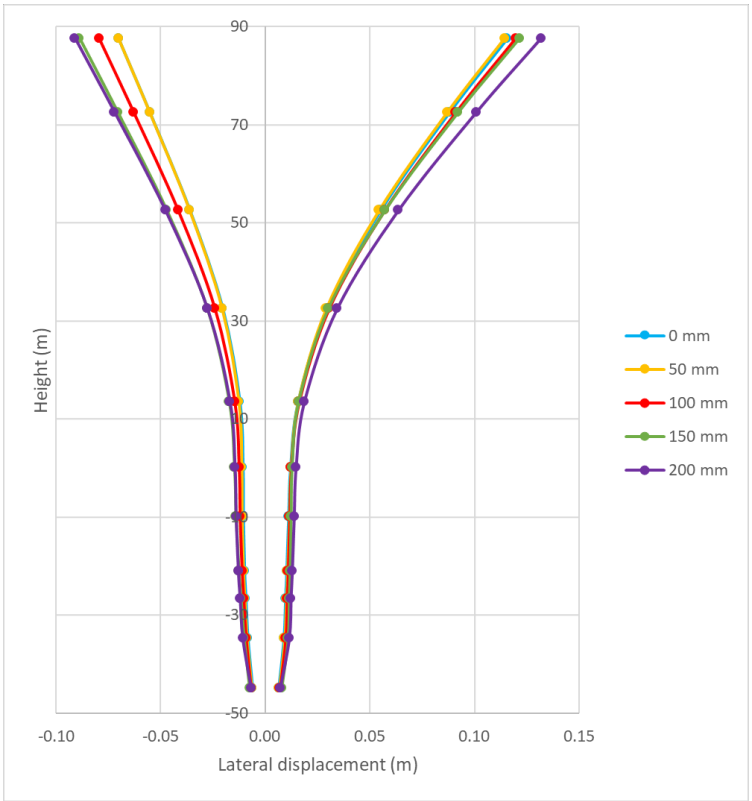

Figure 4 – Along-height lateral displacement Mean+SD and Mean–SD gap visualisation for 5 different marine growth thickness at sea state corresponding to 12 m/s

Table 5 shows a clear trend for lateral displacement mean and SD. The mean values decrease, especially for 100 and 150 mm MG thickness scenarios. Instead, SD values are increased up to 24%. Being one order of magnitude higher than mean values, SD increment has been judged more critical.

A comparison of these results to the ones reported in [29], which refer to a jacket support structure, highlights that the values (maxima ensemble-average) measured on the jacket are up to five times larger than the Mean+SD displacements values on the tripod. In this work, the maxima ensemble average has been computed, for each seed (then averaged again to obtain single value). The maxima have sampled every 10 seconds simulated, for a total of 60 values for each simulation. The interval for the sampling operation has been chosen consistently with the waves peak spectral period. Table 6 helps to evaluate the entity of the difference between the plotted values (Mean+SD) and the 60 maxima average.

Given the nature of the displayed statistics, it is possible to assume that the averaged maxima represent a better mean of comparison. Still, the values found indicate a smaller tower displacement for the tripod support than for the jacket.

Table 5 – Averaged lateral displacement mean and SD % variation for 12 m/s wind speed sea state

MG thickness [mm]	50	100	150	200
% Mean variation	-10.6	-39.6	-89.6	-18.7
% SD variation	+1.2	+8.1	+18.3	+23.9

Table 6 – Comparison of Mean+SD and 60 maximum values average for 3 different positions along the tripod tower height. The case reported refer to 200 mm marine growth thickness and 12 m/s wind speed

	Pile head [m]	**Tower base [m]**	**Tower top [m]**
Mean+SD	0.007	0.015	0.132
60 Maxima Average	0.031	0.053	0.371

Horizontal wave loads

In the simulations, the hydrodynamic loads are computed instantaneously, based on surface elevation. The total wave load acting on the structure increases as the marine growth's layers of the tripod are thicker (Figure 5). As expected, the increased members' diameters cause the surface exposed to the waves to be larger. Consequently, the resulting stress on the structure increases since the additional diameter is not considered as a structural component, being constituted by biofouling.

Base shear

Marine growth does not seem to affect the mean base shear when the turbine is operational, as displayed in Figure 6. Mean values remain constant for 6, 12 and 24 m/s wind speed and increases for 45 m/s. A cause can be found in the different contribution of turbine thrust and wave load to the resulting base shear. While the aerodynamic thrust is largely constant for a given wind speed, the wave load is oscillatory in nature, and increases with marine growth – furthermore, the aerodynamic thrust is, in general, an order of magnitude higher than the surge wave load amplitude. Therefore, a higher turbine thrust contribution (higher than the one of wave load) would justify the nearly constant values as thickness changes. A confirmation can be found on the trend observed as the turbine is not operating:

333 at 45 m/s wind speed the mean base shear clearly increases from 0 to 200 mm thickness scenario. The same trend can be found for
334 standard deviation (Figure 6), meaning, again, an increased probability of high base shear values as marine growth layers thicken.
335

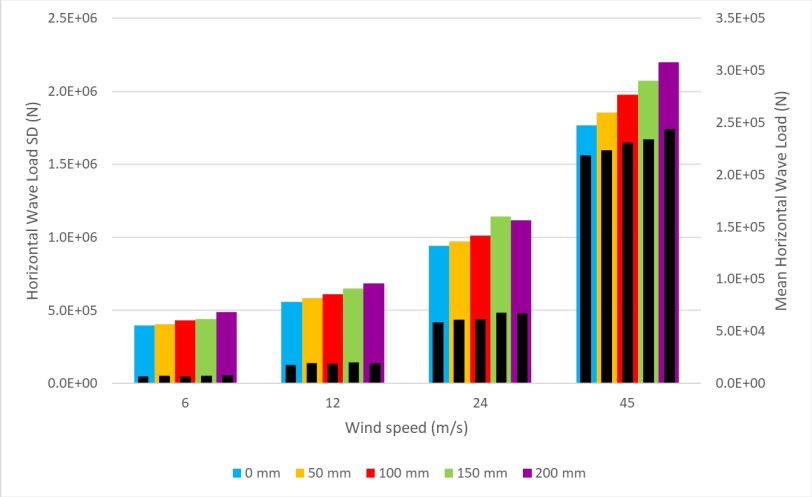

336

337 **Figure 5** – Wave load mean values (black bars) and SD for 5 different values of marine growth thickness and 4 wind speeds

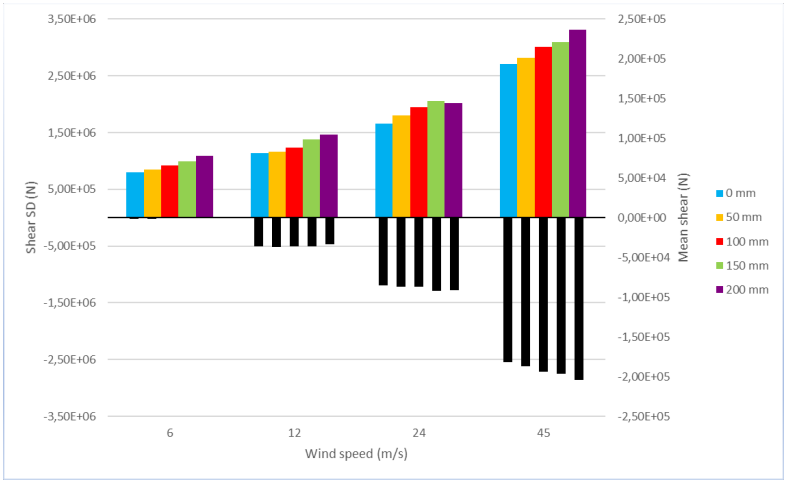

338

339

340 **Figure 6** – Base shear mean values (black bars) and SD for 5 different values of marine growth thickness and 4 wind speeds

341 **Overturning moment**

342 Due to the larger arm (i.e. distance from the seabed level), the rotor thrust provides the largest contribution to the overturning moment
343 (i.e. moment in pitch), which is an estimate of the external forces multiplied by the distance from the soil. This can be observed in Figure

7, where when the turbine is operating, the overturning moment (OT) is almost constant for the different thicknesses simulated, while when the turbine is parked (not operating), the values themselves are lower (when going from 24 to 45 m/s) and strongly affected by the thickness settings, since they are largely due to the oscillatory nature of the wave loads. In fact, by calculating the two separate moments, it is possible to appreciate how, while the mean values belong to the same order of magnitude, the maximum hydrodynamic moment is five times larger than the aerodynamic one.

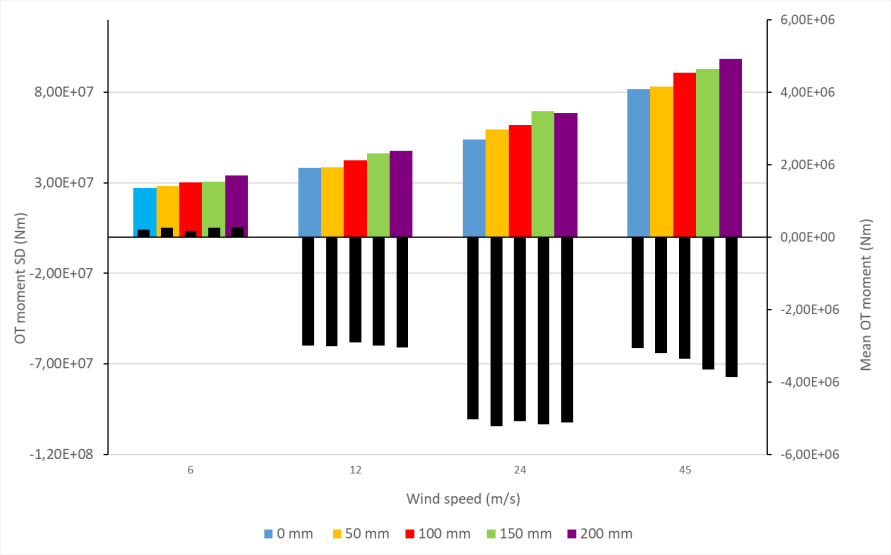

Figure 7 – OT moment mean values (black bars) and SD (colours) for 5 different values of marine growth thickness and 4 wind speeds

4.1.2 Marine growth roughness

The C_M and C_D coefficients have been varied, along the depth, in function of the different characteristics of the MG at different depths, and this had an impact on the loads. It can be seen from Figure 8 that the choice of the default values, causes an overestimation of the mean wave load for every sea state simulated. Being the default values used in case of smooth structure, the overestimation is intended with respect to the "smooth" scenario in which the coefficients have been instead computed as explained in section 3.4.3. The relative overestimation of the standard deviation follows the percentages shown in Table 7.

The difference is larger at low wind speeds (low H_S): for the 6 m/s case it reaches 45%, while for the other wind speeds its magnitude is almost four time smaller (around 10%). This difference comes from the values used in USFOS by default (C_D=0.7 and C_M=2; with respect to those, C_D is the parameter that changes the most comnsidering its dependence from Reynolds and K-C numbers.

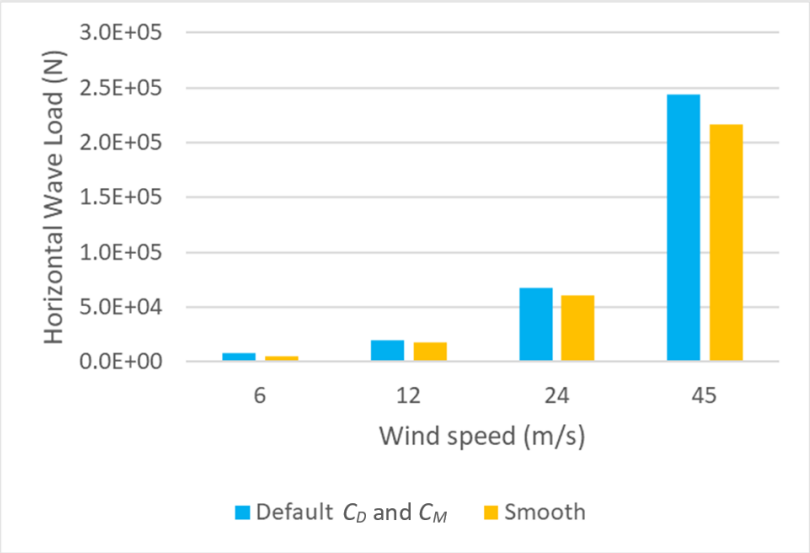

Figure 8 – Mean wave load for 4 sea states when using the default USFOS values or the corrected inertia and drag coefficients

Table 7 – Wave loads when using USFOS default C_D and C_M in place of the corrected ones and percent overestimation

Wind [m/s]	"Default" scenario load [kN]	"Smooth" scenario load [kN]	% Overestimation
6	8.2	5.6	44.5
12	19.6	18.0	8.9
24	67.3	60.7	10.8
45	243.8	216.9	12.4

Sea states dominated by drag forces are represented by high K-C numbers. For these scenarios, C_D is a function of Reynolds number [45]. Normally, a high K-C number can be found close to the water surface, decreasing with depth. The regions below the threshold of K-C=5 [45] are mostly dominated by inertia forces, with drag influence being almost negligible. For sea states with low wind speed (low H_S), then, only the region close to the water surface is characterised by high water velocities. Setting C_D at 0.7 for the whole depth results in a consistent overestimation of the values at low wind speeds because of the low Reynolds number. This can be seen for 6 m/s wind speed scenario, which is not high enough to justify the C_D=0.7 as prescribed by DNV [44] and used in USFOS as default. Instead, for the other sea states the overestimation is smaller. This is mainly due to the C_D values, which are larger than 0.7 because of the high

wind speed and the consequently more severe sea state. Moreover, C_M is nearly the same as the USFOS default one for the whole depth for the other three scenarios.

Figure 9 displays the total wave load experienced by the structure as the marine growth roughness varies. As shown, when roughness increases, also the mean wave load becomes higher. The percent increment with respect to the smooth case is summarised in Table 8. The values are larger when passing from low to high H_S.

The standard deviation is higher for the "Smooth" than for the "5 mm" and "50 mm" roughness scenarios. This result suggests that the inertia dominated conditions (smooth case) cause a larger scatter of load values than the drag dominated ones.

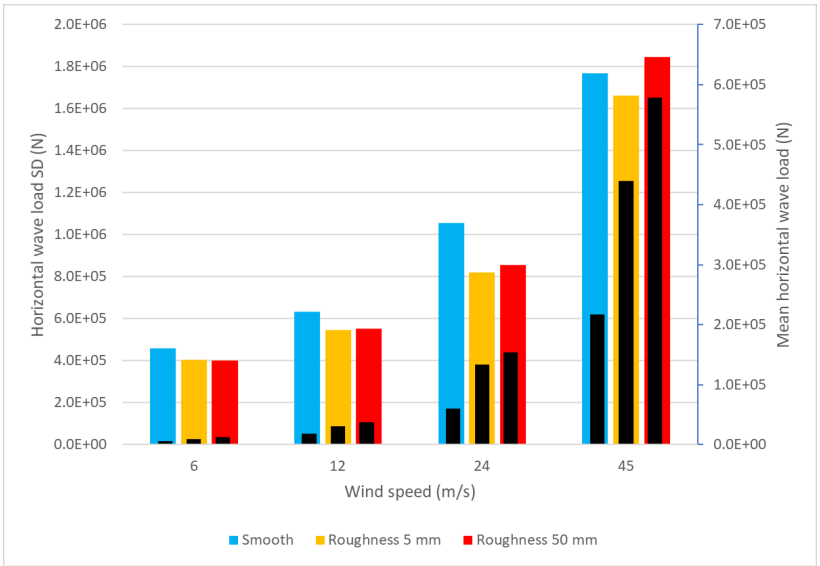

Figure 9 – Wave load mean values (black bars) and SD for 3 different values of MG roughness and 4 wind speeds

Table 8 – Percent mean wave load increase for roughness k=5 mm and k=50 mm with respect to the "Smooth" case

Wind [m/s]	***k* = 5 mm**	***k* = 50 mm**
6	75%	121%
12	70%	111%
24	120%	154%
45	103%	167%

4.1.3 Marine growth non-uniform distribution

The distributions prescribed by the four references considered (Wolfram [39], DNV [7], MID [40], Oldfield [41]) have been set with the desired accuracy mainly on the tower central member, discretised with various cylindrical elements to reproduce its conic shape. Instead, the three long and thin oblique members are discretised with fewer cylindrical members by USFOS and thus the accuracy is not homogeneous for the whole tower. However, the results have been presented because the loads on the central part of the structure are the driving loads when evaluating the structure dynamic behaviour. The outcomes of the simulations correspond to a different marine growth mass added to the "nude" structure. This makes unequal the conditions at which the results would be compared. In fact, while the change in mass does not significantly affect the results, the added volume has been seen to be fundamental for the loads magnitude (as already observed for the constant thickness impact analysis). Therefore, the added volume for each scenario has been calculated, as reported in Table 9.

Table 9 – Mass, additional mass and additional volume for 4 marine growth distributions

	Wolfram [39]	DNV [7]	MID [40]	Oldfield [41]
Mass [tons]	3085	2869	3138	2726
Additional Mass [tons]	715	499	767	356
Additional MG Volume [m^3]	698	487	749	348

Base shear and total wave load show a very similar behaviour when assessing the effect of MG distribution. Therefore, these two will be discussed together and generically referred to as "load". Figure 10 shows base shear's mean and standard deviation when changing marine growth thickness profile along the depth, at 12 m/s. The distributions leading to higher loads are the ones prescribed by Wolfram [39] (1.42 MN) and MID [40] (1.41 MN).

However, even though its lower standard deviation indicate that it would not cause the highest load, the marine growth profile taken from DNV [7] presents a higher mean value (-35 kN). In addition, the added volume is considerably lower: 30 and 35 % less that the first two distribution cited, suggesting that for the same added volume this marine growth profile would cause the loads to be way higher than the others.

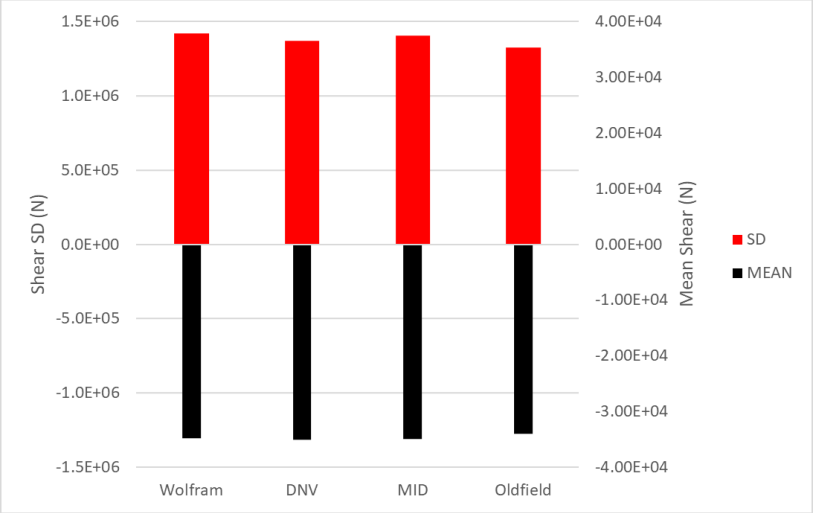

Figure 10 – Mean and SD base shear for 4 marine growth distributions at 12 m/s

4.2 Natural frequencies and structure response in frequency

4.2.1 Natural frequencies analysis

The natural undamped frequencies have been computed using USFOS. The general formula for natural frequencies of a one degree of freedom system is reported (Equation 3), to remind the dependency from the mass, which remains for more complex systems.

$$f = \frac{1}{2\pi}\sqrt{\frac{k}{m}} \tag{3}$$

Differences arise when considering the structure as fixed (Approach A) or when modelling the soil (Approach B). It is possible to appreciate how, in both the approaches (presented in Figure 11 and Figure 12) the first two natural frequencies are not significantly influenced by the presence of marine growth. In terms of design criteria, in fact, the most critical eigen modes have to remain non-excited by the rotor frequency to not cause the phenomenon of resonance, which would greatly enhance the amplitude of the tower oscillation. As explained by Van der Tempel and Molenaar [46], offshore wind turbines are usually designed so that first natural frequency (the tower lateral bending frequency) is far from the 1P and 3P rotor frequency ranges. Given the dimensions of a 5 MW NREL OWT, the "soft-stiff design" is adopted. As a consequence, the first natural frequency has to remain in the middle between the 1P and 3P frequency ranges.

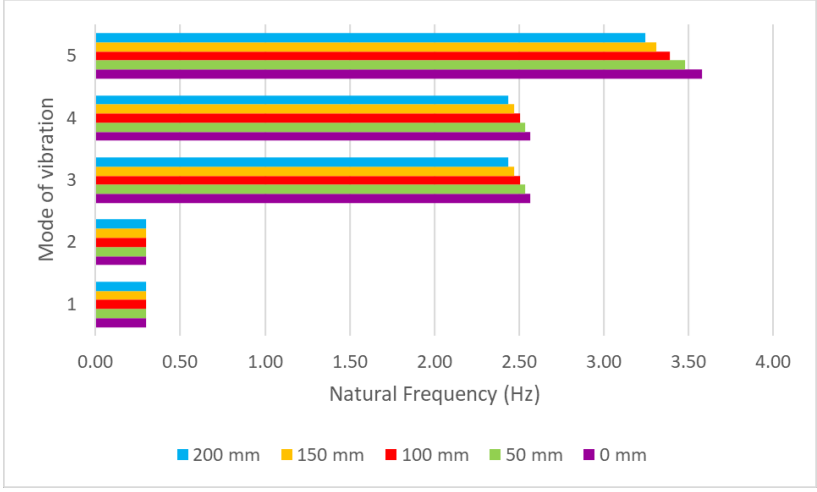

Figure 11 – First 5 modes of vibration natural frequencies for different marine growth thicknesses with Approach A (no soil dynamics modelling)

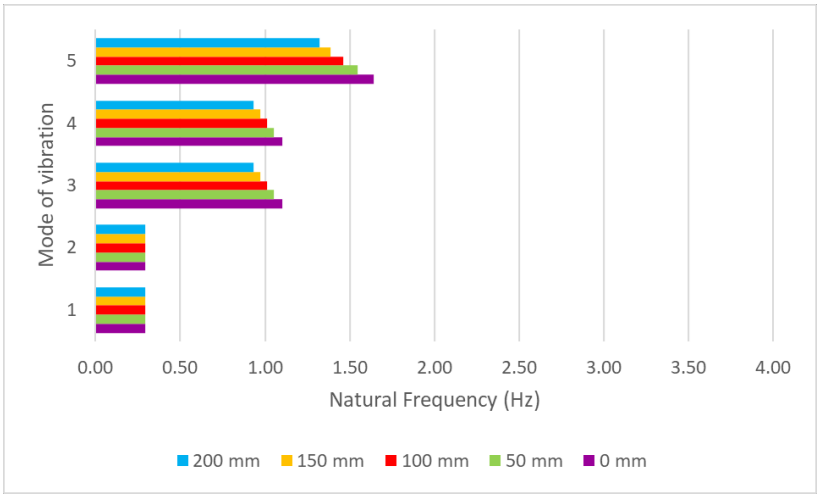

Figure 12 – First 5 modes of vibration natural frequencies for different marine growth thicknesses with Approach B (soil dynamics modelling included)

A different representation of the first two natural frequencies variation is given in Table 10, which compares the percent change with respect to the case with null thickness.

For both the conditions, the variation of first and second modes is nearly negligible. Moreover, as a confirmation of the results obtained, the change is consistent with Fevåg [5]: first and second global natural frequencies are not influenced by the presence of marine growth.

Table 11 shows the comparison between the results of the two studies. The order of magnitude of the results is the same but with a different sign. A decreasing trend would have been expected because of the increment of the total mass of the structure. For example, passing from 150 mm to 200 mm MG thickness, the percent change decreases. The anomalous behaviour is manifesting due to the presence of the soil, making the structure's behaviour to be not linear [14].

Third, fourth and fifth natural frequencies are following the expected trend. As marine growth layers become thicker, the frequency decreases. The added mass in fact, following Equation 3, lowers the frequency. It has also been observed that for higher order natural frequencies the decrement, for thicker MG layers, is more pronounced.

It has also been found that the frequencies that vary the most with the presence of marine growth are the ones which corresponds to an eigen mode that involves a wide movement of the lower part of the structure, which is colonised by marine growth. The first two modes of vibration are characterised by the bending of the upper part of the tower. Consequently, marine growth does not vary these natural frequencies. On the other hand, as the modes of vibrations become more complex, they involve the lower part of the structure:

here the lower members bend and twist. Therefore, the correspondent eigen frequencies' variation is wider. This observation can be appreciated for the first 20 modes of vibration, as presented in Figure 13.

Table 10 – Percent change of the first two natural frequencies with respect to null thickness

	50 mm	**100 mm**	**150 mm**	**200 mm**
	Bottom fixed – Approach A			
1	-0.08%	-0.15%	-0.19%	-0.17%
2	-0.08%	-0.15%	-0.19%	-0.17%
3	-1.08%	-2.2%7	-3.57%	-4.97%
4	-1.08%	-2.27%	-3.57%	-4.97%
5	-2.82%	-5.30%	-7.46%	-9.34%
	Loose sand soil – Approach B			
1	0.17%	0.29%	0.290%	0.16%
2	0.17%	0.29%	0.290%	0.16%
3	-4.25%	-8.16%	-11.77%	-15.11%
4	-4.25%	-8.16%	-11.77%	-15.11%
5	-5.71%	-10.76%	-15.28%	-19.36%

Table 11 – First natural frequency percent variation comparison between the present study and [5]

	Present study	**[5]**
50 mm	0.17%	0.0%
100 mm	0.29%	-0.1%
150 mm	0.29%	-0.2%
200 mm	0.16%	-0.3%

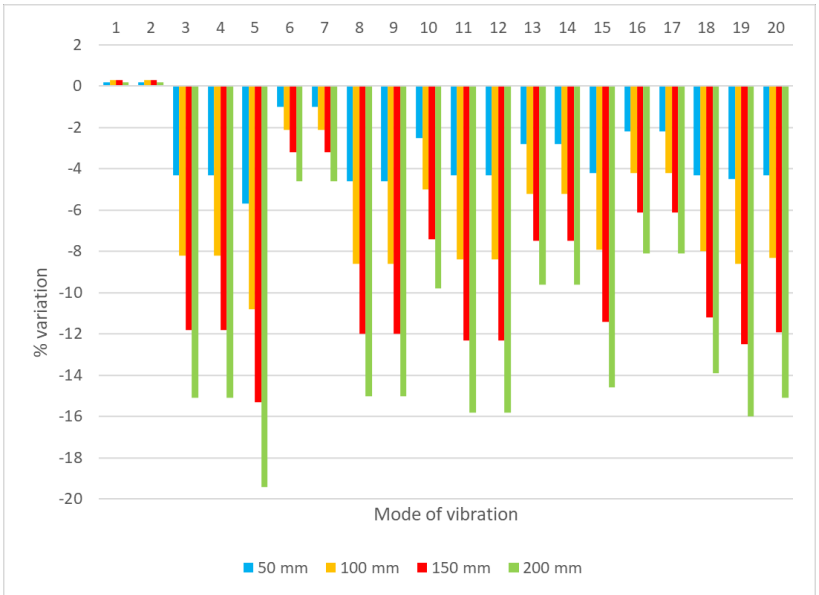

458

459 **Figure 13** – Relative variation for the first 20 natural frequencies as MG thickness increases

460

461 *4.2.2 Comparison of the natural and exciting frequencies*

462 Wind loads spectra are across a low range of frequencies (Bhattacharya [47]), and therefore out of the resonance range. Following
463 the analysis made by Fevåg [5], it can be said that also the wave load spectrum peak frequency (around 0.1 Hz for a 10 m/s peak spectral
464 period sea state) is substantially lower than the modes of vibration natural frequencies of the structure, first of which is set at 0.29 Hz.
465 Then, it is not expected that the wave loads will substantially excite the structural modes of vibration. Anyway, a bit of structural
466 oscillation is present, therefore the contribution of the wave loads to the horizontal oscillatory displacement is tangible.

467 Table 12 summarises the exciting frequencies due to the turbine rotational motion. The rotation speed gives the 1P frequency, which
468 is the most critical one together with 3P (the blade passing frequency for a three-bladed wind turbine).

469 By comparing of the values summarised in Figure 12 (bar chart of natural frequencies) and the ones in Table 12, it is possible to
470 confirm that neither the 1P nor the 3P turbine rotational frequencies cause resonance. Given the value of the tripod first natural frequency,
471 0.293 Hz, which lays into the gap 1P-3P for each wind speed, the safe design of the structure can be confirmed to be the soft-stiff [46].

472

473

474

475 **Table 12 –** Turbine rotation frequencies at each wind speed

Wind speed [m/s]	**Rotor speed [rpm]**	**Excitation frequency [Hz]**			
		1P	**3P**	**6P**	**9P**
6	7.9	0.132	0.395	0.79	1.185
12	12.1	0.202	0.605	1.21	1.815
24	12.1	0.202	0.605	1.21	1.815
45 (parked turbine)	0	0	0	0	0

476

477

478 *4.2.3 Response frequency spectra*

479 In order to better understand the impact of the marine growth thickness on the dynamic response of the OWT, it is useful to analyse
480 the changes in the lateral displacement response spectrum when the amount of biofouling is changed.

481 Figure 14 shows a shift in the third peak frequency for the different scenarios. This is caused by structure's mass change for the
482 different marine growth thicknesses. Since the increased thickness enlarges the members' diameter as well, a simple method to assess
483 the impact of the two phenomena on the natural frequencies change is here proposed.

484 In order to confirm that the shift in frequencies may be due to the change in mass, an equivalent but approximated 1 DOF system
485 model is used. This approach simplifies consistently the dependency from mass in such a complex system but can provide a useful
486 insight and confirmation.

487 The values presented in Table 13 are displayed as percent of relative variation. It can be observed that the expected values are very
488 close to the actual values obtained by extracting them from the frequency spectra. Then, it can be confirmed that the peak shifts
489 accordingly to the mass increase due to the marine growth thickness increment.

490

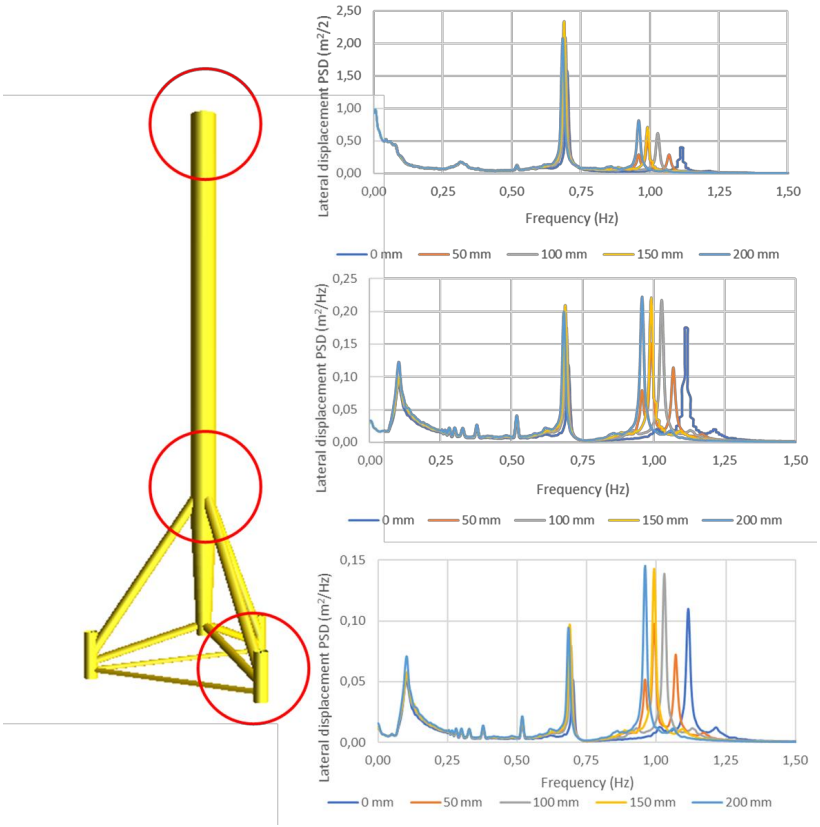

491

492 **Figure 14** – From top to bottom: tower top, tower base and pile head lateral displacement response frequency spectra for 12 m/s load case,

493 for 5 different MG thickness values

494

495

496 **Table 13 –** Expected and actual percent peak relative distance for 5 marine growth densities and thicknesses (at 12 m/s wind speed)

	Thickness [mm]				
	0	**50**	**100**	**150**	**200**
Mass [tons]	2370	2580	2800	3035	3280
Frequency expected % variation		-4.3	-8.7	-13.2	-17.6
Peak Frequency [Hz]	1.114	1.07	1.028	0.992	0.96
Peak frequency actual % shift		3.9	7.7	11.0	13.8

497

Figure 15 highlights how the wave load experienced by the structure increases in intensity: the increment is 19% passing from 0 to 200 mm marine growth thickness. However, the exciting frequency does not change.

By comparing the structure's response frequency spectra at different heights along the tower (Figure 14), some key trends have been discovered. Firstly, the wave load excitation frequency (always close to 0.1 Hz) can be found in the structure's response only in the submerged parts and not in the tower top response spectrum, as expected. Moreover, the peak at 0.7 Hz, caused by the wind load, increases of importance passing from the pile head (near the seabed), to the tower base, and to the tower top, where it corresponds to the highest value. Therefore, the parts of the structure excited mainly from just one of the two types of load will present, as expected, a higher peak at the frequency of that excitement source. It is also possible to identify a minor peak set at 0.3 Hz. This is the first natural frequency of the structure, at which the tower oscillates due to the free from constraints top end. The peak is emphasised at 45 m/s, as shown in Figure 16, because the parked wind turbine condition makes the tower to behave just as a simple cantiliver, having just one end constrained in all its degrees of freedom. Therefore, the tower vibrates at its natural frequency at its free end.

The trends and observations made for the frequency spectra shown are similar for all the other sea states that have been simulated for the study. The comparison of Figure 14 and Figure 16 highlights that the third peaks are characterized by just one maximum in the 45 m/s scenarios, while a more variable shape is identifiable for the other loading cases. The cause has been found in the average operation This suggests that, as the turbine passes to the parked configuration, the system simulated by the software is simpler, having all the turbine's controls disabled.

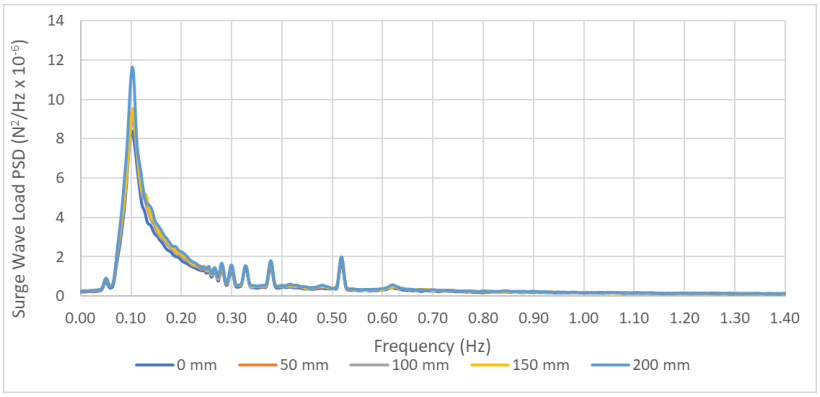

Figure 15 – Total wave load frequency spectra for 6 m/s sea state for 5 different MG thickness values

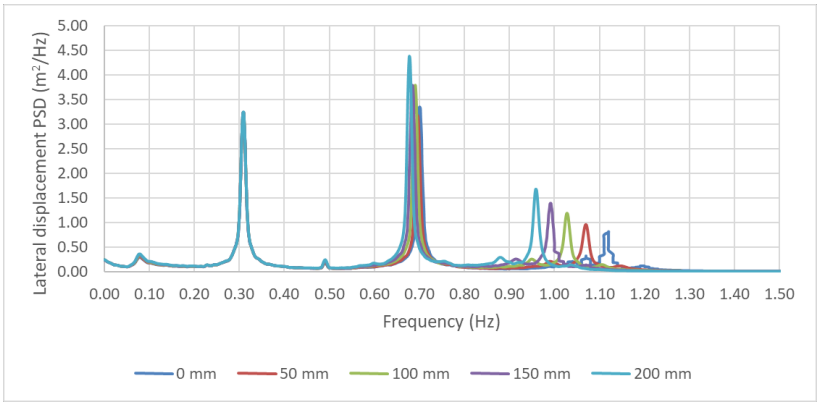

Figure 16 – Tower top response frequency spectra for 5 marine growth thicknesses at 45 m/s wind speed

5. CONCLUSIONS

Offshore wind turbines represent a proven solution for producing renewable energy on a vast scale. This technology poses additional design challenges as well as the need of careful maintenance planning. So far, there have been few attempts to investigate the influence of marine growth on the response of fixed offshore wind turbine structures, especially on offshore wind turbines utilising a tripod structure as support structure, and considering the soil-structure interaction. Therefore, in the present work a methodology and the results of an aero-hydro-servo-geo-elastic dynamics analysis is given, discussing the impact of the marine growth thickness and roughness on the dynamic response of the system.

The main findings can be summarized as:

- Increase of loads on the tripod for an increasing marine growth thickness;
- Importance of roughness modelling, since the results are highly sensitive to this parameter;
- Absence of variation for the critical natural frequencies (first two modes) in any scenario;
- Discrepancy between the guidelines of the different codes.

Lateral displacement and loads increase as marine growth thickens. Furthermore, different thickness profiles and different roughness values have shown to have a clear impact as well.

Thickness variation has a high impact both on loads and structure's lateral displacement: the standard deviation increases up to 24% for 200 mm MG thickness, meaning a higher probability of wider tower oscillations. Indeed, due to the increased diameter of the braces, the wave load experienced by the structure is enhanced. It is noticeable that the tripod support seems to experience smaller displacement than the jacket one. While the base shear and overturning moment are not heavily affected when the turbine is operational, these are

539 increasing as marine growth thickens. Marine growth thickness distribution along the structure required a comparison that considered
540 the effectively added volume, the cause of the enlarged loads. Furthermore, the marine growth profile prescribed by DNV has been
541 identified as the most critical, given the high loads and low added volume if compared to the other non-homogeous distributions.

542 The analysis on the impact of the roughness revealed to induce a reduction of the wave loads in the case of smooth marine growth.
543 In fact, using the values automatically set by USFOS [48] causes a significant overestimation especially at low wind speeds, where sea
544 states are mainly dominated by drag forces. When roughness is increased, the enhanced drag coefficient causes larger wave load and
545 base shear. Mean values increases up to 167% (nearly 60 kN) of the "smooth" scenario.

546 The natural frequency analysis has clearly shown a decreasing trend due to the mass increment. Nevertheless, the first two natural
547 frequencies demonstrated a negligible change (0.3%), but still at the designed soft-stiff conditions between 1P and 3P rotor frequency
548 ranges. The peaks identified through the frequency spectra analysis have shown no sign of resonance. As marine growth thickens, the
549 third peak's frequency is lower. It has been pointed out, though, how the tower top oscillates at the first natural frequency given its
550 freedom from constraints. The origin of the peaks has been determined with a prior analysis of the effect of the single loading conditions:
551 while the 0.1 Hz peak represents the response to the wave load, the peak spotted at 0.7 Hz is caused by the wind. The third peak shifting
552 trend has been identified as mass-connected. In fact, the relative frequency decrement is in line with the predicted one, computed
553 considering the 1 DOF system mass dependency.

554 Then, it has been observed that the references for marine growth thickness profiles can lead to added volume differences up to 35 %
555 between each other. This finding underlines the necessity to considerate the appropriate profile for each marine envronment for accurate
556 load calulations.

557 However, it is worth highlighting that the work here presented has shown two main limitations. Firstly, the effect of the distributions
558 (of thickness and hydrodynamic coefficients) could be better appreciated with a smaller discretization of the lower part of the tripod
559 structure. The adjustment would make USFOS to assign the values with higher accuracy, respecting the desired profile. Secondly, the
560 non-linearity due to the soil modelling, displayed when computing the natural frequency of the structure, could be explained and
561 therefore confirmed by using a software implementing a different soil model. Both limitations will be the topic of future research carried
562 out by the authors.

563

564

ACKNOWLEDGEMENTS

The authors wish to express their gratitude to Tore Holmas of www.usfos.no for his help with the finite element program for framed offshore structures, USFOS.

REFERENCES

[1] X. Wang, X. Zeng, J. Li, X. Yang, and H. Wang, A review on recent advancements of substructures for offshore wind turbines, *Energy Conversion and Management*, 158, 2018, 103–119. https://doi.org/10.1016/j.enconman.2017.12.061

[2] WindEurope, Offshore Wind in Europe - Key trends and statistics - 2017, www.windeurope.org, 2018. https://doi.org/10.15713/ins.mmj.3

[3] E. Lozano-Minguez, A. J. Kolios, and F. P. Brennan, Multi-criteria assessment of offshore wind turbine support structures, *Renewable Energy*, 36 (11), 2011, 2831–2837. https://doi.org/10.1016/j.renene.2011.04.020.

[4] B. C. O'Kelly and M. Arshad, Offshore wind turbine foundations - analysis and design, in C. Ng and L. Ran (eds.), *Offshore Wind Farms - Technologies, Design and Operation*, Elsevier, 2016, 589–610. https://doi.org/10.1016/B978-0-08-100779-2.00020-9.

[5] L. S. Fevåg, Influence of marine growth on support structure design for offshore wind turbines, *Masters Thesis*, Norwegian University of Science and Technology (NTNU), Trondheim, Norway, 2012.

[6] W. Shi, H.-C. Park, J.-H. Baek, C.-W. Kim, Y.-C. Kim, and H.-K. Shin, Study on the marine growth effect on the dynamic response of offshore wind turbines, *International Journal of Precision Engineering and Manufacturing*, 13 (7), 2012, 1167–1176. https://doi.org/10.1007/s12541-012-0155-7

[7] DNV, Offshore Standard-DNV-OS-J101 – Design of Offshore Wind Turbine Structures, Det Norske Veritas AS, 2014.

[8] A. M. Al-Yacouby, V. J. Kurian, A. A. Sebastian, M. S. Liew and V. G. Idichandy, Effects of marine growth on hydrodynamic ccoefficients of rigid tubular cylinders, *Applied Mechanics and Materials*, 567, 2014, 247–252. https://doi.org/10.4028/www.scientific.net/AMM.567.247.

[9] E. L. Nedrebø, Experimental investigation of marine fouling on piles in currents, *Masters Thesis*, Norwegian University of Science and Technology (NTNU), Trondheim, Norway, 2014.

[10] T. Sarpkaya, N. J. Collins, and S. R. Evans, Wave forces on rough-walled cylinders at high Reynolds numbers, *Proceedings of the Offshore Technology Conference (OTC)*, 1977, 175–184. https://doi.org/10.4043/2901-MS.

591 [11] W. Carswell, Soil-structure modeling and design considerations for offshore wind turbine monopile foundations, *PhD Thesis*,
592 University of Massachusetts Amherst, 2015.

593 [12] K. A. Abhinav and N. Saha, Dynamic analysis of an offshore wind turbine including soil effects, *Procedia Engineering*, 116,
594 2015, 32–39. https://doi.org/10.1016/j.proeng.2015.08.261.

595 [13] S. Bisoi and S. Haldar, Dynamic analysis of offshore wind turbine in clay considering soil-monopile-tower interaction, *Soil*
596 *Dynamics and Earthquake Engineering*, 63, 2014, 19–35. https://doi.org/10.1016/j.soildyn.2014.03.006.

597 [14] K. A. Abhinav and N. Saha, Nonlinear dynamical behaviour of jacket supported offshore wind turbines in loose sand, *Marine*
598 *Structures*, 57, 2018, pp. 133–151, 2018. https://doi.org/10.1016/j.marstruc.2017.10.002.

599 [15] Karimirad, M. and T. Moan (2011). Wave-and wind-induced dynamic response of a spar-type offshore wind turbine. Journal
600 of Waterway, Port, Coastal, and Ocean Engineering, 138(1), 9–20.

601 [16] J. Jonkman and W. Musial, Offshore code comparison collaboration (OC3) for IEA task 23 offshore wind technology and
602 deployment, *Technical Report NREL/TP-5000-48191*, National Renewable Energy Laboratory, Golden, Colorado. 2010.
603 https://doi.org/NREL/TP-5000-48191.

604 [17] P. S. Veers, Three-dimensional wind simulation, *Technical Report SAND88-0152*, Sandia National Laboratories, Albuquerque,
605 USA, 1988.

606 [18] J. M. Jonkman and M. L. Buhl Jr., FAST – User's guide, *Technical Report NREL/EL-500-38230*, National Renewable Energy
607 Laboratory, Golden, Colorado, 2005.

608 [19] Martin O. L. Hansen, Aerodynamics of Wind Turbines, Earthscan, 2007.

609 [20] J. M. Jonkman, G. J. Hayman, B. J. Jonkman, and R. R. Damiani, AeroDyn v15 User's Guide and Theory Manual, *Technical*
610 *Report*, National Renewable Energy Laboratory, Golden, Colorado, 2015.

611 [21] SINTEF, USFOS – Getting Started. Structural Engineering, SINTEF, Marintek. 2001.

612 [22] J. R. Morison, M. P. O'Brien, J. W. Johnson, and S. A. Schaaf, The force exerted by surface waves on piles, *Petroleum*
613 *Transactions*, 189, 1950, 149–154. https://doi.org/10.2118/950149-G.

614 [23] N. Saha, Z. Gao and T. Moan, Sampling uncertainty of simulated stochastic waves and response process of a vertical cylinder
615 fixed to sea-bed, *Proceedings of the 8th International Conference on Structural Dynamics, EURODYN 2011*, Leuven, Belgium, 3408–

3415.

[24] T.H. Søreide, J. Amdahl, E. Eberg, T. Holmås and Ø. Hellan, USFOS-a Computer Program for Progressive Collapse Analysis of Steel Offshore Structures. Theory Manual, SINTEF, 1993.

[25] L.C. and W. van Impe, Single Piles and Pile Groups under Lateral Loading, CRC Press, 2011.

[26] P. le Tirant, Offshore Pile Design, Editions Technip, 1992.

[27] API-RP2A-WSD, APIRP - 2A - WSD Recommended practice for planning, designing and constructing fixed offshore platforms–working stress design. API Publishing Services, 2000. https://doi.org/10.1007/s13398-014-0173-7.2.

[28] D. Zwick and M. Muskulus, The simulation error caused by input loading variability in offshore wind turbine structural analysis, *Wind Energy*, 18 (8), 2015, 1421–1432. https://doi.org/10.1002/we.1767.

[29] K. A. Abhinav and N. Saha, Stochastic response of jacket supported offshore wind turbines for varying soil parameters, *Renewable Energy*, 101, 2017, 550–564. https://doi.org/10.1016/j.renene.2016.09.019.

[30] Damiani, R., Wendt, F., Finucane, Z., Hulliger, L., Chilka, S. and Dolan, D. 2018, Assessment of Sequentially vs. Fully Coupled Dynamic Analysis of Offshore Wind Turbines, *Technical Report - NREL/TP-5000-68618, National Renewable Energy Laboratory, Golden, Co*.

[31] Z. Gao, N. Saha, T. Moan, and J. Amdahl, Dynamic analysis of offshore fixed wind turbines under wind and wave loads using alternative computer codes, *Proceedings of the 3rd Conference on the Science of making Torque from Wind*, Crete, Greece, 2010.

[32] Passon, P. and Branner, K. 2014, Load calculation methods for offshore wind turbine foundations, *Ships and Offshore Structures, 9(4), pp.433-449*.

[33] M. Seidel, M. Von Mutius, and D. Steudel, "Design and load calculations for offshore foundations of a 5 MW turbine," *Proceedings of the 7th German Wind Energy Conference DEWEK*, Wilhelmshaven, Germany, 2004, 351-356.

[34] U. Yukio and S. M. H. Rashed, The idealized structural unit method and its application to deep girder structures, *Computers and Structures*, 18 (2), 1984, 277–293. https://doi.org/10.1016/0045-7949(84)90126-3.

[35] J. K. Paik and A. K. Thayamballi, A concise introduction to the idealized structural unit method for nonlinear analysis of large plated structures and its application, *Thin-Walled Structures*, 41 (4), 2003, 329–355. https://doi.org/10.1016/S0263-8231(02)00113-1.

[36] DNV GL, SESAM GeniE User Manual. Concept design and analysis of offshore structures, Vol. 1, DNV GL AS, 2011.

[37] K. Johannessen, T.S. Meling and S. Haver, Joint distribution for wind and waves in the northern North Sea, *International Journal of Offshore and Polar Engineering*, 12 (1), 2002.

[38] M. A. Carswell, W, Arwade, S. R, DeGroot, D. J and Lackner, Soil–structure reliability of offshore wind turbine monopile foundations, *Wind Energy*, 18 (3), 2015, 483–498.

[39] J. Wolfram, "The effect of marine growth on vortex shedding and fatigue life of tubular members: Results from a case study," *Proceedings of the First International Offshore and Polar Engineering Conference (ISOPE)*, Edinburgh, United Kingdom, 1991.

[40] MTDL, Appraisal of Marine Growth on Offshore Installation, Marine Technology Directorate Limited, 1992.

[41] D. G. Oldfield, Appraisal on Marine Fouling on Offshore Structures, *Offshore Technology Paper*, CIRIA, 1980.

[42] T. Van Der Stap, J. W. P. Coolen, and H. J. Lindeboom, "Marine fouling assemblages on offshore gas platforms in the southern North Sea: Effects of depth and distance from shore on biodiversity," *PLOS One*, 11 (1), 2016. https://doi.org/10.1371/journal.pone.0146324.

[43] M. A. El-Reedy, Offshore structures: Design, construction and maintenance, Gulf Professional Publishing, 2012.

[44] DNV, Recommended Practice-DNV-RP-C205 – Environmental conditions and environmental loads, Det Norske Veritas AS, 2010. https://doi.org/10.1109/INTLEC.1993.388591.

[45] M H Patel, Dynamics of Offshore Structures, Butterworth-Heinemann, 1989.

[46] J. van der Tempel and D.-P. Molenaar, Wind turbine structural dynamics – A review of the principles for modern power generation, onshore and offshore, *Wind Engineering*, 26 (4), 2002, 211–222. https://doi.org/10.1260/030952402321039412.

[47] S. Bhattacharya, J. A. Cox, D. Lombardi, and D. Muir Wood, Dynamics of offshore wind turbines supported on two foundations, *Proceedings of the Institution of Civil Engineers-Geotechnical Engineering*, 166 (2), 2013, 159–169. https://doi.org/10.1680/geng.11.00015.

[48] SINTEF. USFOS Hydrodynamics – Theory, Description of use, Verification, SINTEF, Marintek, 2010.